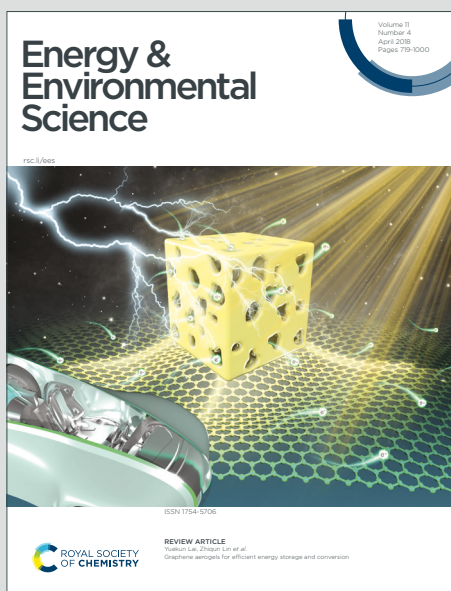


Energy & Environmental Science

Accepted Manuscript

This article can be cited before page numbers have been issued, to do this please use: J. Holoubek, K. Kim, Y. Yin, Z. Wu, H. Liu, M. Li, A. Chen, H. Gao, G. Cai, T. A. Pascal, P. Liu and Z. Chen, *Energy Environ. Sci.*, 2022, DOI: 10.1039/D1EE03422G.



This is an Accepted Manuscript, which has been through the Royal Society of Chemistry peer review process and has been accepted for publication.

Accepted Manuscripts are published online shortly after acceptance, before technical editing, formatting and proof reading. Using this free service, authors can make their results available to the community, in citable form, before we publish the edited article. We will replace this Accepted Manuscript with the edited and formatted Advance Article as soon as it is available.

You can find more information about Accepted Manuscripts in the [Information for Authors](#).

Please note that technical editing may introduce minor changes to the text and/or graphics, which may alter content. The journal's standard [Terms & Conditions](#) and the [Ethical guidelines](#) still apply. In no event shall the Royal Society of Chemistry be held responsible for any errors or omissions in this Accepted Manuscript or any consequences arising from the use of any information it contains.

Electrochemical kinetics and their temperature dependence play a vital role in the performance and environmental operating limitations of high-energy batteries. Technologically, the kinetic limitations of standard cell chemistries preclude the cycling of Li metal batteries at sub-zero temperatures, which suffer a severe reduction in reversibility of plating and stripping and catastrophic shorting events due to dendritic growth. The limitations of secondary batteries in these temperature ranges have been proposed to be limited by the ion-desolvation penalty faced by Li^+ at the electrolyte/electrode interphase, for which few methods of optimization exist. In this work, we demonstrate the importance of ion-pairing between Li^+ and the anion within the electrolyte to low-temperature operation through a systematic study. In doing so, we demonstrate homogenous Li metal deposition, highly-reversible plating and stripping, and hundreds of stable cycles in > 4 V Li metal full batteries down to -40 °C in an electrolyte system that would otherwise catastrophically fail under the same conditions without said ion-pairing in the solvation sphere. This work endeavors to unambiguously demonstrate the importance of solvation structure engineering in lithium battery electrolytes designed for operation under kinetic stress.

1 **Electrolyte Design Implications of Ion-Pairing in Low-Temperature Li Metal**
2 **Batteries**

3 John Holoubek^a, Kangwoon Kim^b, Yijie Yin^b, Zhaohui Wu^c, Haodong Liu^a, Mingqian Li^c,
4 Amanda Chen^c, Hongpeng Gao^b, Guorui Cai^a, Tod A. Pascal^{a,b,c,d,*}, Ping Liu^{a,b,c,d,*}, Zheng
5 Chen^{a,b,c,d,*}

6 ^a*Department of NanoEngineering, University of California, San Diego, La Jolla, CA 92093, USA*

7 ^b*Program of Materials Science, University of California, San Diego, La Jolla, CA 92093, USA*

8 ^c*Program of Chemical Engineering, University of California, San Diego, La Jolla, CA 92093, USA*

9 ^d*Sustainable Power and Energy Center, University of California, San Diego, La Jolla, CA 92093,*
10 *USA*

11 Abstract

12 *Lithium metal batteries are capable of pushing cell energy densities beyond what is*
13 *currently achievable with commercial Li-ion cells and are the ideal technology for supplying*
14 *power to electronic devices at low temperatures (≤ -20 °C). To minimize the thermal management*
15 *requirements of these devices, batteries capable of both charging and discharging at these*
16 *temperatures are highly desirable. Here, we report > 4 V Li metal full cell batteries (N/P=2)*
17 *capable of hundreds of stable cycles down to -40 °C, unambiguously enabled by the introduction*
18 *of cation/anion pairs in the electrolyte. Via controlled experimental and computational*
19 *investigations in electrolytes employing 1,2-dimethoxyethane as the solvating solvent, we observed*
20 *distinct performance transitions in low temperature electrochemical performance, coincident with*
21 *a shift in the Li^+ binding environment. The performance advantages of heavily ion-paired*
22 *electrolytes were found to apply to both cathode and anode, providing Li metal Coulombic*
23 *efficiencies of 98.9, 98.5, and 96.9 % at -20 , -40 , and -60 °C, respectively, while improving the*
24 *oxidative stability in support of > 4 V cathodes. This work reveals a strong correlation between*
25 *ion-pairing and low-temperature performance while providing a viable route to Li metal full*
26 *batteries cycling under extreme conditions.*

28 Introduction

29 The advent of Li-ion batteries (LIBs) has enabled the rapid development of advanced
30 portable electronics and electric vehicles. However, the application of existing and next-generation
31 electronic devices in extremely low temperatures (< -20 °C) is currently limited by a significant
32 reduction in the energy density of LIBs under such conditions.^[1-5] Li metal batteries (LMBs),
33 which replace the graphite anode (372 mAh g^{-1}) with Li metal (3860 mAh g^{-1}) have gathered recent
34 interest to improve cell-level energy density, and if realized would be the ideal technology for low-
35 temperature devices.^[6] However, LMBs are known to face poor cycling stability due to the
36 inherent reactivity and volume change of the Li metal anode. These factors present as a low
37 Coulombic efficiency (CE) during repeated plating and stripping and may result in dendritic Li
38 growth which may penetrate the battery separator and short the cell.^[7,8] What's more, cycling of
39 the Li metal anode under sub-zero conditions further exacerbate these effects.^[9-11] To overcome
40 these challenges, significant advancements in battery engineering and a scientific understanding
41 of these devices and their temperature scaling is crucial.

42 To address the capacity and voltage loss experienced by secondary batteries at low
43 temperature, engineering of the electrolyte chemistry has emerged as a promising tool.^[8-16] Though
44 there has been much progress in the improvement of low temperature battery performance, most
45 works have focused on the improvement of low temperature discharge following a charge at
46 benign temperatures.^[2,4,15,16] Unless the device employing such batteries can be removed from the
47 cold operating environment during charge, this operation protocol inherently couples the designed
48 battery to an external warming device. These warming systems consume non-negligible power and
49 contribute mass to the overall system, thus reducing overall operating efficiency and energy
50 density.^[17,18] For applications that must be charged in their working environment, enabling low
51 temperature charge and discharge is necessary to reduce or eliminate the need for thermal
52 management at low temperature. For LMBs, this implies that Li metal must be reversibly plated
53 and stripped under these conditions.

54 Along with technological progress, a more rigorous understanding of the interplay between
55 various limiting factors at low temperature is necessary. Historically, improving the bulk ionic
56 conductivity, solid-electrolyte interphase (SEI) composition, and Li⁺ charge-transfer penalty have
57 been the foremost goals of low temperature electrolyte design.^[3,4, 9-11,19-21] Among these factors, it
58 has been suggested that the charge-transfer penalty is the dominant limitation among systems with
59 sufficient bulk transport.^[2,22,23] However, the heterogenous charge-transfer process in
60 electrochemical systems is invariably complicated, particularly given that there is no mechanistic
61 consensus regarding Li⁺ dynamics at the electrode interphase in the presence of a SEI. While it is
62 clear that factors such as SEI composition, Li⁺ solvation structure, and interphasial dynamics play
63 important roles in this process, their influence on one another is largely unknown. Hence, the
64 technological advancement of temperature-resilient energy storage is heavily linked to a
65 fundamental understanding of the charge-transfer process.

66 Our previous work aimed to provide low temperature system design principles based on
67 the hypothesis that the solvation environment of the Li⁺ ion in the electrolyte defines the charge-
68 transfer barrier and its temperature dependence.^[23] While we demonstrated state-of-the art Li metal
69 reversibility down to -60 °C, the design insights gleaned from the LMB electrolyte of interest
70 raised many questions that have yet to be answered. It was concluded that solvents of weak Li⁺
71 binding were crucial to advantageous temperature scaling of Li metal reversibility, which agrees

72 with the results from Li et al.^[22], Fan et al.^[16], and Wang et al.^[24]. However, such weak binding
73 solvents commonly result in Li⁺/anion binding in bulk solution, making a direct correlation
74 between low temperature performance and any one factor difficult. This work aims to decouple
75 the influence of ion-pairing and Li⁺/solvent binding energy to gain a more definitive sub-zero LMB
76 electrolyte design rationale and provide further insights on the temperature dependence of charge-
77 transfer.

78 To provide such data, we propose a detailed comparison of electrolytes composed of the
79 same solvating solvent with varying degrees of ion-pairing. The most direct way to accomplish
80 this would be varying the solvating solvent/Li salt ratio.^[25-27] However, the high viscosity of such
81 electrolytes make this untenable when scaling to low temperatures, where any advantage in
82 interphasial charge-transfer kinetics would be completely obscured by the overwhelming decrease
83 in ionic conductivity.^[16] Fortunately, a solution to this already exists in the advent of localized
84 high-concentration electrolytes (LHCEs). These systems apply diluent solvents, which interact
85 weakly with Li⁺ and dissolve negligible salt on their own, in order to reduce the bulk viscosity of
86 high-concentration electrolytes.^[28-30] In doing so, any effects of ion-pairing in the Li⁺ solvation
87 shell can be decoupled from the bulk ionic conductivity of the solution at low temperature. LHCEs
88 employing 1,2-dimethoxyethane (DME) was chosen as the primary basis of this investigation. This
89 solvent has been well established to provide reversible room temperature Li metal performance
90 when paired with lithium bis(fluoro sulfonyl)imide (LiFSI), even at dilute concentrations.
91 However, the temperature dependence of Li reversibility is demonstrably acute^[23,31,32], which we
92 and others have proposed to be linked to its strong binding with Li⁺. Thus we pair the LiFSI/DME
93 components with a bis(2,2,2 trifluoro ethyl)ether (BTFE) diluent, which allows for the modulation
94 of the degree of ion-pairing while maintaining a relatively low bulk viscosity. We incrementally
95 alter the BTFE/DME volume ratio from 1 M LiFSI in pure DME to 1 M LiFSI BTFE/DME (7:1,
96 8 M equivalent local concentration). Using both theoretical and experimental methods, we
97 demonstrate that there is a distinct ion-pairing transition when the local concentration exceeds 4
98 M (3:1 BTFE/DME ratio), which results in vastly improved Li metal performance at low
99 temperatures, while improving the oxidative stability and thus enabling the implementation of
100 LiNi_{0.8}Mn_{0.1}Co_{0.1}O₂ (NMC 811) as a cathode material. This concept was utilized to design LMBs
101 capable of charging *and* discharging at low temperatures, as illustrated in Figure 1.

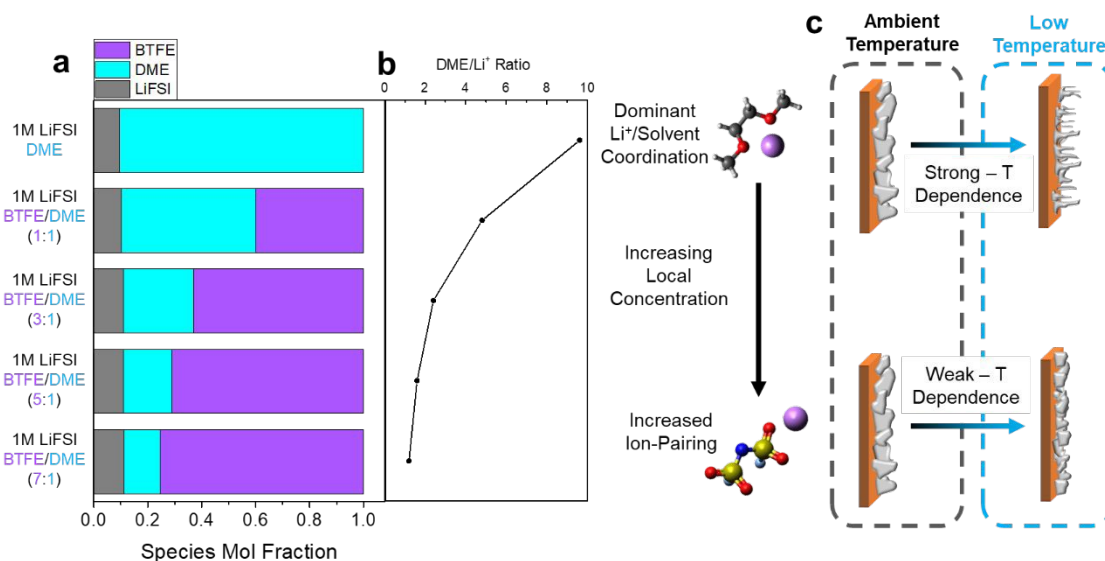


Figure 1. Overview of **a)** electrolytes of interest and their molar composition, **b)** coincident effect of molar DME/Li⁺ ratio on ion-pairing in solution, and **c)** the effect of these factors on the temperature dependence of Li cycling.

102

103 To provide a basis for the assessment of low temperature Li metal performance and the
 104 eventual design of LMB full batteries, physical characterization of the DME-based electrolytes of
 105 interest was first conducted. Though our previous results have indicated exceptional ionic
 106 conductivity is not necessarily a prerequisite for reversible low temperature Li metal
 107 performance^[23], the freezing of electrolytes and exponential increases in their viscosity is known
 108 to overwhelm electrochemical performance.^[11,21] As shown in Figure 2a, it was confirmed that all
 109 systems of interest remained in a liquid state down to -60 °C. To provide an insight into the effect
 110 of temperature on ionic transport, the ionic conductivities were also measured (Figure 2b). It was
 111 found that the systems of lowest local concentration (i.e., lowest DME/LiFSI ratio but still 1 M
 112 with respect to the total volume of BTFE and DME) displayed far superior transport, where the 1
 113 M LiFSI in DME, 1:1, 3:1, 5:1, and 7:1 BTFE/DME electrolytes displayed ionic conductivities of
 114 15.2, 11.2, 9.18, 3.60, and 2.43 mS cm⁻¹ at 20 °C, respectively. This trend was largely maintained
 115 at low temperature, where the systems retained 6.20, 2.87, 2.54, 0.87, and 0.50 mS cm⁻¹ at -40 °C,
 116 respectively. The reduction of bulk conductivity with increased ion-pairing is well-established,
 117 and can be generally described by a reduction in ionicity due to the strong interactions between
 118 cation and anion.^[28,33] It is also noteworthy that the inclusion of BTFE in the electrolytes were
 119 found to slightly increase the viscosity, where the 1 M LiFSI DME, 1 M LiFSI BTFE/DME (1:1)

120 and 1 M LiFSI BTFE/DME (5:1) electrolytes displayed viscosities of 1.7, 2.7, and 2.4 cP,
121 respectively, however the viscosity of these systems all remains below that of conventional
122 carbonate systems (Figure S1). Although ion-pairing is hypothesized to result in improved charge-
123 transfer kinetics, its tradeoff with bulk transport may indicate that an intermediate concentration
124 may be optimal for low-temperature LMB applications.

125 Electrolytes utilizing DME generally display poor oxidative stability due to the inherent
126 HOMO energy of ether solvents.^[29,34,35] Though these systems are typically applied in Li-S
127 batteries, the low-temperature performance degradation of the S cathode has been observed to be
128 severe, due in large part to clustering processes inherent to the polysulfide conversion process.^[1]
129 As such, transition metal oxide cathode hosts remain to be highly desirable for low temperature
130 applications, which require the oxidative stability of the electrolyte to exceed 4 V vs. Li/Li⁺.
131 Despite its disadvantages for ion transport through the bulk, increased local concentration (and
132 increased ion-pairing) is known to produce advantageous effects on the electrochemical stability
133 of the system.^[25-29] This was found to be the case for the DME-based LHCE systems investigated
134 here as well, where the areal current produced by linear-scan voltammetry (LSV) on an Al current
135 collector was found to exceed 0.02 mA cm⁻² at 4.22, 4.31, 5.34, > 5.5, and > 5.5 V for 1 M LiFSI
136 in DME, 1:1, 3:1, 5:1, and 7:1 BTFE/DME, respectively (Figure 2c). However, it is worth noting
137 that there is a slight increase in oxidative current between 3.7 and 4.5 V within the 3:1 LSV profile,
138 which indicates that a slight decomposition reaction occurs to form a passivating interphase, after
139 which the current decreases again. It was also found that these trends were maintained in the
140 presence of conductive carbon and NMC 811, where 1 M LiFSI DME and 1 M LiFSI BTFE/DME
141 (1:1) showed significantly increased decomposition behavior at lower voltages than their
142 counterparts (Figure S2).

143 The transport and electrochemical stability trends are a direct symptom of increased ion-
144 pairing due to heightened local concentrations (i.e., lower DME/Li⁺ ratio). To observe this
145 experimentally and to serve as an aid to future computational studies, Raman spectroscopy was
146 carried out on the electrolytes of interest and their pure components (Figure 2d). It was found that
147 the S-N-S bending peak of the FSI⁻, present in the salt spectra at 774 cm⁻¹, undergoes a significant
148 shift to 719 cm⁻¹ when dissolved at 1 M in DME, indicative of the separation between Li⁺ and FSI⁻
149 produced by the DME. This peak was then found to progressively shift to 732 cm⁻¹ in the 3:1

150 mixture, which indicates an increase in ion-pairing between Li^+ and FSI^- in solution.^[28] Though the
 151 peak shift between 1 M LiFSI DME and 1 M LiFSI BTFE/DME (3:1) appears to be linear, it is
 152 noteworthy that this shift is substantially heightened between the 3:1 and 5:1 systems.
 153 Additionally, the 5:1 and 7:1 mixtures display much broader S-N-S peaks, indicating an increased
 154 amount of bound FSI^- solvation states within the system. Moreover, a similarly large reduction in
 155 conductivity was observed between the 3:1 and 5:1 mixtures (Figure 2b). This ion-pairing was also
 156 found to result in a slight but incremental increase in Li^+ transference number, from 0.32 in 1 M
 157 LiFSI DME to 0.53 in the 7:1 system (Figure S3). Though this increase is significant, our previous
 158 work indicates that such an increase has little effect on the interphasial Li^+ depletion when
 159 observed in tandem with a reduction of ionic conductivity of such a magnitude.^[23] These
 160 phenomena are further examined in the molecular dynamics analysis below.

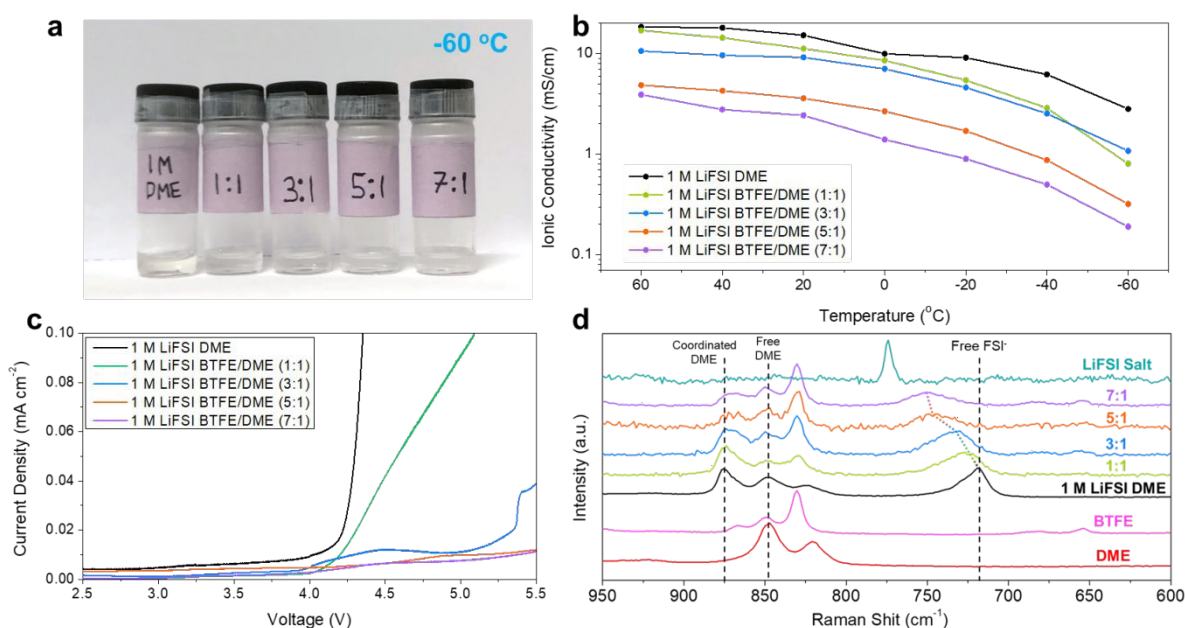


Figure 2. Physical and electrochemical properties of the electrolytes of interest. **a)** Optical photograph of electrolytes at $-60\text{ }^{\circ}\text{C}$. **b)** Measured ionic conductivity across temperature. **c)** Oxidative linear scan voltammetry of selected systems on Al current collectors at 1 mV s^{-1} . **d)** Raman spectra of the electrolytes and their pure

161
 162 To examine the implications of these electrolyte properties on low-temperature LMB
 163 reversibility, the CE of Li plating was determined in Li||Cu cells via the accurate galvanostatic
 164 method proposed by Adams *et al.*^[36] Testing at 23 and $-20\text{ }^{\circ}\text{C}$ was conducted at 0.5 mA cm^{-2}
 165 whereas we used 0.25 mA cm^{-2} for -40 and $-60\text{ }^{\circ}\text{C}$. Due to the intrinsic reductive stability of ether
 166 solvents and the fluorine-donating capabilities of LiFSI, 1 M LiFSI DME, and 1 M LiFSI 1:1, 3:1,

167 5:1, and 7:1 BTFE/DME systems were found to display reversible CEs of 96.0, 99.1, 99.1, 99.4,
168 and 99.4% at room temperature (Figure 3a). These CEs were also found to persist over many
169 plating and stripping cycles (Figure S4). The relatively improved CEs of the electrolytes
170 containing BTFE is likely due to the increased prevalence of fluorine in the SEI layers, which was
171 confirmed via XPS (Figure S5), however the chemical identity of the SEI was found to be
172 relatively similar across systems, which agrees with previous literature.^[37] However, when the
173 temperature was reduced it was found that the scaling of such reversibility was not equal across
174 the systems. In particular, systems of lower local concentration displayed substantial noise in the
175 voltage curves, which can be attributed to soft-shortening events at low temperature and contribute
176 to extremely reduced CEs.^[9,23] Specifically, the 1 M LiFSI DME electrolyte was found to short at
177 -20 °C, whereas the CE of the 1:1 mixture reduced to 94.8% at -20 °C (Figure 3b), before finally
178 shorting at -40 °C. At -40 and -60 °C, the 3:1, 5:1, and 7:1 electrolytes were found to produce
179 reversible CEs of 98.9, 98.5, 98.6, and 96.6, 96.9, 96.4 %, respectively (Figure 3c,d). A summary
180 of these trends is shown in Figure 3e for ease of comparison.

181 Additionally, the critical current for each electrolyte was assessed in Li||Li cells at each
182 temperature. The profiles for these tests are shown in Figure S6, where it was found that the 1 M
183 LiFSI BTFE/DME (5:1) electrolyte maintains critical currents of 5, 3, and 0.75 mA cm⁻² at -20, -
184 40, and -60 °C, which is the highest among the investigated systems. It is also worth noting that
185 the critical current often exceeds the shorting currents observed in Li||Cu tests, which implies that
186 nucleation of Li on Cu also plays a role in the poor performance. Indeed, previous reports have
187 observed a substantial variance in nucleation behavior at reduced temperatures.^[31] A summary of
188 these critical currents is shown in Figure 2f, which provides a basis for safety assessment at the
189 full cell level. Crucially, we note that the optimal electrolytes for low temperature Li metal
190 performance and ionic conductivity do not align, which agrees with previous reports and indicates
191 that the low temperature performance is dictated by charge-transfer.^[22,23]

192

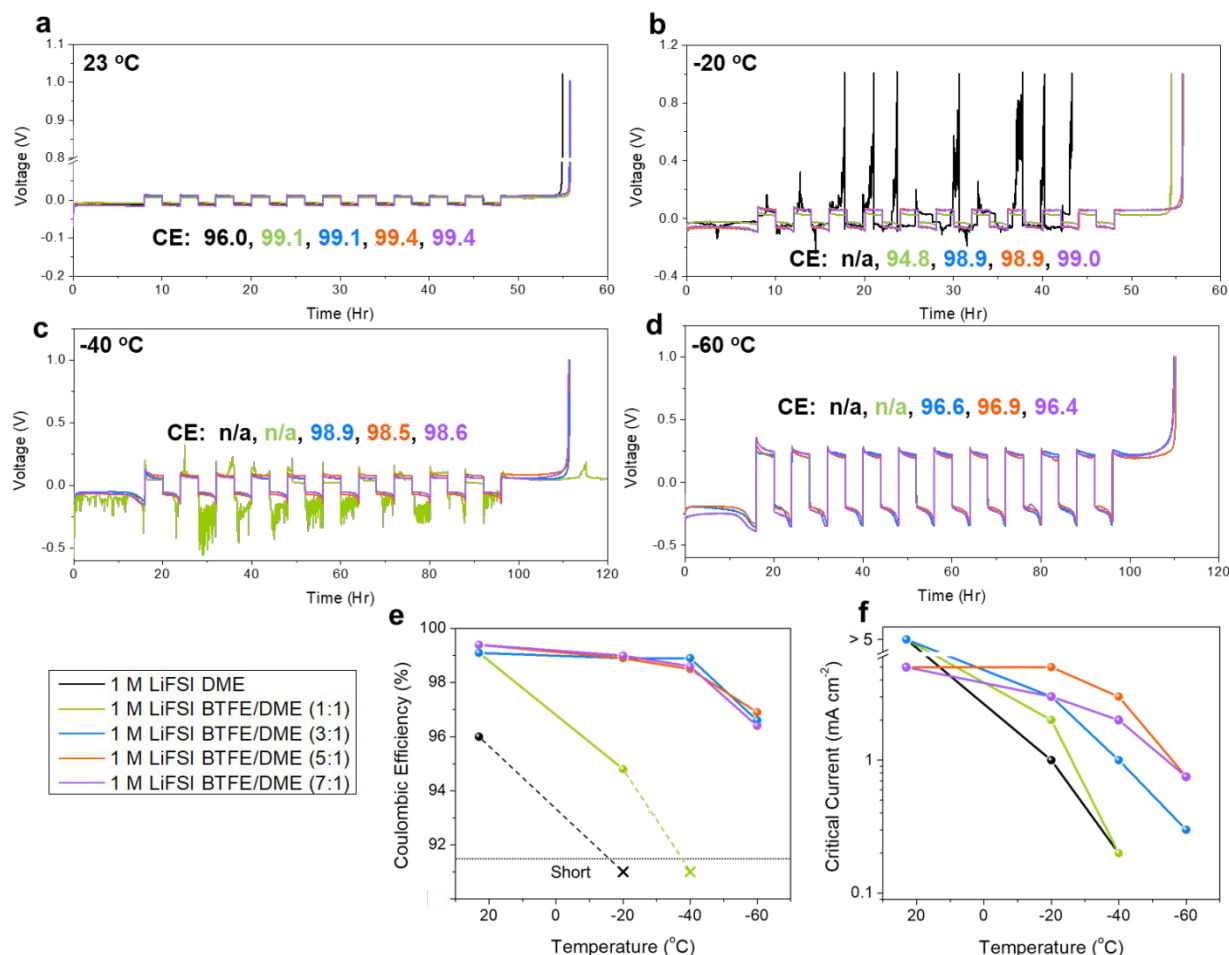


Figure 3. Li metal performance measurements at room and low temperature. Voltage profiles of Li/Cu cells employing electrolytes of interest at **a)** 23 °C and 0.5 mA cm⁻², **b)** -20 °C and 0.5 mA cm⁻², **c)** -40 °C and 0.25 mA cm⁻², **d)** -60 °C and 0.25 mA cm⁻². In all cases a conditioning cycle was conducted and not shown. Summaries of **e)** Coulombic efficiency and **f)** Critical current of the electrolytes of interest at various temperatures.

193

194 To further understand the interplay between ion-pairing and Li metal performance at low
 195 temperature from a morphological standpoint, scanning electron microscopy (SEM) was
 196 conducted on Li deposited on Cu current collectors at 23 and -40 °C. Photographs taken of the Cu
 197 electrodes after deposition at 23 °C reveal metallic Li deposits with a silver appearance, which is
 198 typically indicative of micron-scale Li deposits, as uncontrolled nanoscale morphologies typically
 199 appear black in color (Figure 4a). SEM images of the Li deposited at room temperature confirm
 200 this, where Li was found to deposit in the “chunk” morphology often associated with electrolytes
 201 of similar composition.^[28-30,37] Interestingly, the micro-scale uniformity was found to increase
 202 coincidentally with increasing local concentration. This may be a direct result of the increased
 203 electrochemical stability of the electrolyte associated with higher concentration, where salt driven

204 passivation of the interphase is typically achieved due to the restriction of reactive solvent by the
205 strongly coordinated Li^+ .^[25-29,33-35,37]

206 When carrying out the same deposition process at $-40\text{ }^\circ\text{C}$ we observed a distinct shift in
207 both the macroscopic and microscopic structure, however. Similar to the previously presented data,
208 we believe the origin of this behavior and its asymmetric temperature dependence across systems
209 corresponds to the local concentration of each system and the coincident ion-pairing of their
210 solvation shells. First, it was observed that the amount of Li plated on the Cu current collectors in
211 1 M LiFSI DME and 1 M LiFSI BTFE/DME (1:1) undergoes a severe reduction at $-40\text{ }^\circ\text{C}$. This
212 phenomenon has been observed in our previous work^[23] and is believed to be a direct indication
213 that these systems suffer from severe shorting at low temperature which renders Li plating
214 unnecessary to balance the charge of the electrochemical circuit. Furthermore, bundles of nano-
215 sized dendritic filaments were observed in the 1 M LiFSI DME sample (Figure S7), which may be
216 directly responsible for the shorting behavior. On the other hand, homogenous Li deposition was
217 achieved in 1 M LiFSI BTFE/DME 3:1, 5:1, and 7:1 systems, which agrees with the trends
218 observed in the CE measurements at $-40\text{ }^\circ\text{C}$ and below. Notably, the optimum in terms of deposit
219 size and uniformity at $-40\text{ }^\circ\text{C}$ was produced by 1 M LiFSI BTFE/DME (5:1) instead of the 7:1
220 solution, which may suggest that among systems of comparable charge-transfer kinetics the
221 relatively poor ionic conductivity of the 7:1 electrolyte may be problematic. Despite this, the
222 reduced Li deposition size produced by the 7:1 electrolyte at $-40\text{ }^\circ\text{C}$ did not result in a clear
223 reduction in CE relative to the 3:1 and 5:1 electrolytes, which is likely related to the inherently
224 lower reactivity of this heavily ion-paired system. We have also observed dendritic growth in the
225 Li deposits produced by 1 M LiFSI BTFE/DME (1:1) at $-20\text{ }^\circ\text{C}$, which coincides with a substantial
226 decrease in CE despite the lack of soft-shortening phenomena (Figure S8). Such dendritic growth
227 was also found to result in a significant increase in plated Li porosity, where 4 mAh cm^{-2} of plated
228 Li was found to exhibit thicknesses of 32.7, 25.3, 22.6, and 23.2 μm for 1 M LiFSI BTFE/DME
229 (1:1), (3:1), (5:1), and (7:1), respectively (Figure S9).

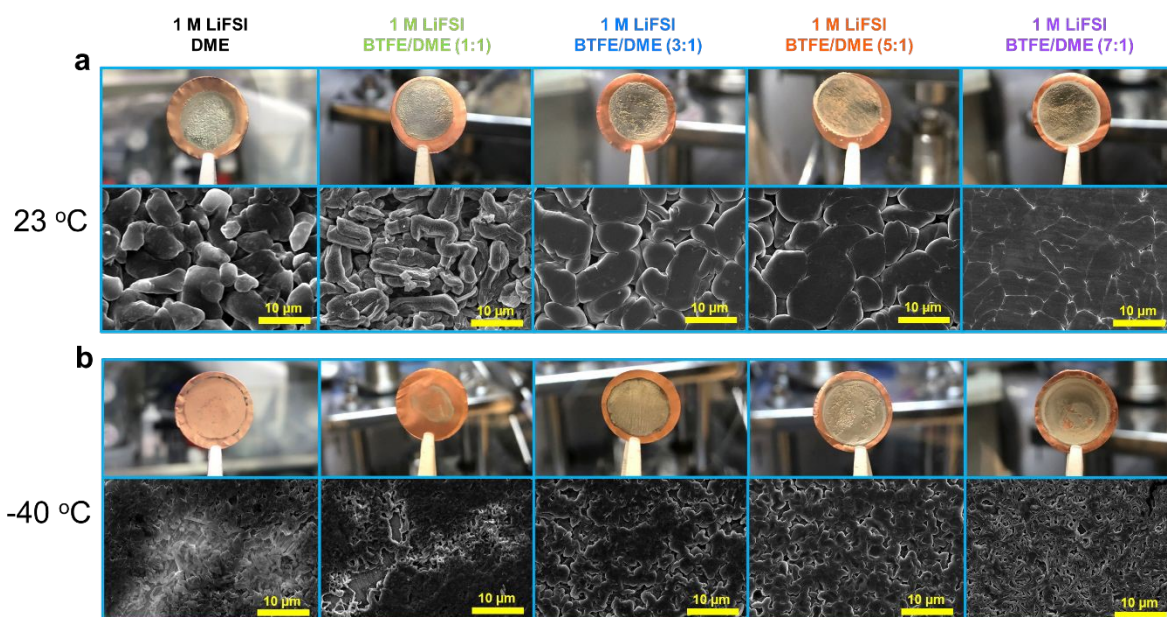


Figure 4. Characterization of Li metal deposits in electrolytes of interest. Optical and SEM photographs of 5 mAh cm^{-2} of Li metal deposited at **a)** $23 \text{ }^\circ\text{C}$ and **b)** $-40 \text{ }^\circ\text{C}$. All depositions were carried out at 0.5 mA cm^{-2} .

230

231 As previously discussed, the charge-transfer barrier is thought to be the limiting factor at
232 low temperatures. Such behavior and its temperature dependence is defined by the inner and outer-
233 sphere reorganization energies (further discussed below), themselves defined by the solvation
234 environment of Li^+ in solution.^[22,38-42] To understand this microscopic solvation structure in the
235 LHCE systems, we performed classical MD simulations. Here, ~ 500 total molecules were
236 assembled in various ratios of Li^+ , FSI⁻, DME, and BTFE, depending on the electrolyte in question
237 (Table S1), and subjected to 25 ns of production dynamics after initial equilibration, from which
238 the solvation data were extracted. A more detailed description of these simulations is provided in
239 the Supporting Information. Representative snapshots from the MD simulations can be found in
240 Figure 5a, where it can be seen that the spatial distribution of the ions shift substantially as the
241 concentration increases. At the highest DME/ Li^+ ratio (9.6:1) found in 1 M LiFSI DME, the Li^+
242 ions are distributed homogeneously in solution. However, at the higher local concentrations found
243 in the 3:1 electrolyte and above, significant aggregation of solvating clusters composed of Li^+ , FSI⁻
244 and DME separated by regions of BTFE was found. This local aggregation effect is also observed
245 in a previous ab-initio MD work^[43], and partially accounts for the reduced ionic conductivity of
246 the systems with high local concentrations. The stochastic trajectory of the Li^+ ion over the 25 ns
247 is presented in Figure S11 to visualize the effect of aggregation on ionic motion. We reason that

248 this effect is a symptom of the disparate solvating power of DME and BTFE, where the Li^+ ion far
249 prefers interaction with the former, forming ion-pairs as the amount of available DME
250 decreases.^[28]

251 To quantify the local environment around the Li^+ ion in solution, the radial distribution
252 function (RDF) with respect to Li^+ was calculated. Figure 5b,c shows the RDF due to the oxygens
253 of DME and FSI^- respectively, and the associated integrals (i.e. the coordination number) is shown
254 in Figure 5d and e. This analysis revealed that 1 M LiFSI in DME largely prefers a solvent-
255 separated ion-pair structure (SSIP), in which the Li^+ is coordinated only by solvent in the first
256 solvation shell. Our previous work has noted that the DME dominated SSIP solvation environment
257 is correlated with poor low temperature performance.^[23] However, with increasing local
258 concentration (increased BTFE/DME ratio) the DME in the primary solvation shell was
259 sequentially displaced by FSI^- molecules, such that the average coordination of environments of
260 the 1 M LiFSI DME and 7:1 electrolytes were calculated to be $\text{Li}^+(\text{DME-O})_{5.0}(\text{FSI-O})_{0.3}$ and
261 $\text{Li}^+(\text{DME-O})_{3.0}(\text{FSI-O})_{2.5}$, respectively. BTFE was not found to solvate Li^+ in any statistically
262 significant manner (Figure S12), which is also supported by the Raman spectra (Figure 2d). It is
263 noteworthy that there is generally a distinction made between different ion-paired states, where
264 one coordinating FSI^- per Li^+ is typically deemed a “contact-ion-pair” (CIP), while FSI^-
265 coordination numbers > 1 are denoted as an “aggregate” (AGG).^[26] In this regard, the RDF data
266 suggests that SSIP, CIP, and AGG structures dominate as the local concentrations increases.

267 Though the RDF data reveals the *average solvation structure*, in this case, they fail to
268 properly describe the *distribution* of solvation states the Li^+ takes in each system. To explore this,
269 250 snapshots of each Li^+ and its local environment were extracted for each simulation (between
270 10,750 and 12,500 snapshots depending on the simulation) and tabulated (Supporting
271 Information). In this analysis, we adopted the naming convention “X-Y-Z” to denote the number
272 of DME (X), FSI^- (Y), and BTFE (Z) found within the first solvation shell of Li (within 3 Å). It
273 was found that the 1 M LiFSI DME electrolyte most prominently displayed a local environment
274 of 3-0-0 (68.5 %), with a lower prevalence of 2-1-0 (27.8 %) which correspond to SSIP and
275 contact-ion-pair (CIP) solvation environments, respectively. More moderate local concentrations
276 (e.g., 3:1) were found to be dominated by CIP, while the higher concentrations tended to prefer
277 AGG states. Though the calculated Li^+ transference numbers indicate that the MD simulations
278 may slightly exaggerate the ion-pairing character of these systems, this trend is maintained (Figure

279 S3). Representative structures for each system are shown in Figure 2f, and alternatively displayed
 280 in Figure S12f. Consistent with our previous work,^[23] we now elaborate on how the CIP/aggregate
 281 dominated systems are advantageous at low temperatures.

282

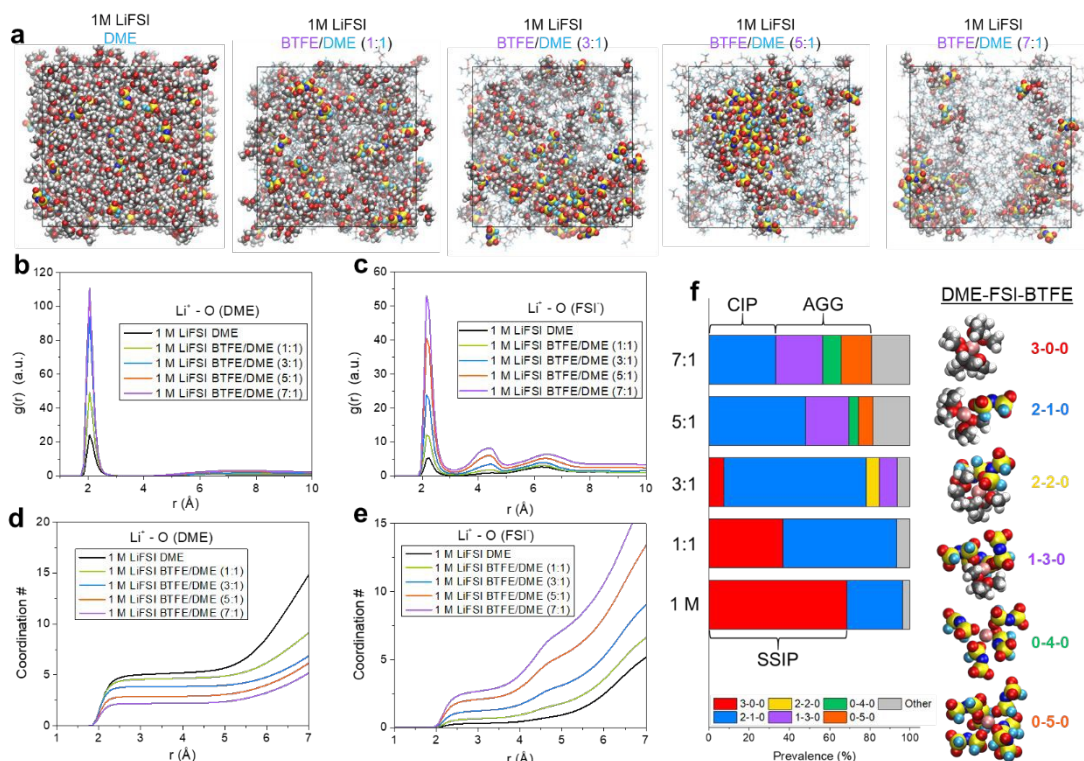


Figure 5. Molecular dynamics analysis of electrolytes of interest. **a)** Snapshots of MD simulations. Radial distribution functions of **b)** DME and **c)** FSI⁻ oxygens with respect to Li⁺. Coordination numbers of **d)** DME and **e)** FSI⁻ oxygens with respect to Li⁺. **f)** Solvation structure distribution analysis of systems of interest and representative MD snapshot of each significant coordination environment.

283

284 It has been widely observed that charge transfer impedance at low temperatures
 285 overwhelms and thus dictates the performance of Li-based batteries at low temperatures, which
 286 we have recently hypothesized to be the cause of the dendritic growth and subsequent shorting of
 287 LMBs under such conditions.^[2,22,23] The experimental and theoretical evidence presented in this
 288 work establishes a more robust correlation between ion-pairing and improved Li reversibility at
 289 low temperature. While this information is practically useful for low temperature electrolyte
 290 design, it is crucial to note that a causal string has not yet been identified. The temperature
 291 dependence of charge-transfer in Li-based batteries is a complicated topic that undoubtedly

292 warrants further study, however there are a number of recent works that may provide additional
293 insights into the phenomena observed here.

294 To gain further insights into the charge-transfer phenomena, we take a perspective based
295 on Marcus Theory. This framework and its subsequent iterations are generally thought to be the
296 most accurate model of electrochemical kinetics at the interphase, and have recently been
297 demonstrated to accurately describe Li metal plating.^[38-42,44] Perhaps the most relevant parameter
298 to our work, which partially defines both the adiabaticity and energy of the transition state is the
299 reorganization parameter λ , which generally consists of inner-sphere and outer-sphere
300 components. The former describes the reorganization energy of the electronic structure and
301 vibrational modes within the solvation sphere, while the latter describes the energetic cost of
302 nuclear motion (i.e., deformation) of the coordinating species. To interpret the results presented
303 here, and in keeping with previous studies^[39-41], it is generally assumed that inner-sphere
304 reorganization is largely temperature *independent*, whereas outer-sphere reorganization is
305 significantly temperature *dependent*.

306 The effect of ion-pairing on these reorganization factors has been typically studied in a
307 variety of electrochemical systems, where it has been suggested that increased pairing results in
308 improved outer-sphere energetics.^[45,46] In aprotic media, the formation of ion-pairs in the double
309 layer has been proposed to allow the cation to approach the interphase at smaller distances than
310 SSIP structures^[46], which preliminary quantum chemistry results indicate may be the case in this
311 work, where FSI- removal was found to be unlikely when compared to DME removal (Figure S13).
312 It is also worth noting that different degrees of ion pairing were found to display different behavior
313 at said interphases, which may also describe the variance in performance between the 3:1, 5:1, and
314 7:1 electrolytes.^[46] However, recent work from Boyle et al. indicates that these conclusions may
315 not directly translate to improved Li metal kinetics at room temperature.^[44] This work found that
316 though the interphasial impedance was substantially lowered by the introduction of ion-pairs, the
317 reorganization parameter underwent little change. We hypothesize that this is a direct result of an
318 increased contribution from e^- transfer resistance (i.e. inner-sphere) to the total reorganization
319 energy in ion-paired systems. Additionally, the presence of ion-pairing was also concluded to
320 reduce the electronic coupling between the electrode and Li^+ , which may be a direct result of
321 increased binding energy between Li^+ and the anion (Figure S13). While this reduced coupling is

322 broadly detrimental to charge-transfer, the nature of electronic phenomena suggests it has little
 323 influence on temperature dependent performance. Considering the temperature dependence of
 324 inner and outer-sphere reorganization, these results would predict that the increased ion pairing in
 325 our systems gives rise to similar behavior at room temperature, but leads to disparate scaling at
 326 low temperatures, consistent with our experimental findings. Further, our model is supported by
 327 the recent work from Wang et al., which suggested that electrolytes dominated by Li^+/DME
 328 interactions have a particularly large entropy of Li/Li^+ exchange, which is incrementally reduced
 329 by the introduction of ion-pairing in solution.^[32]

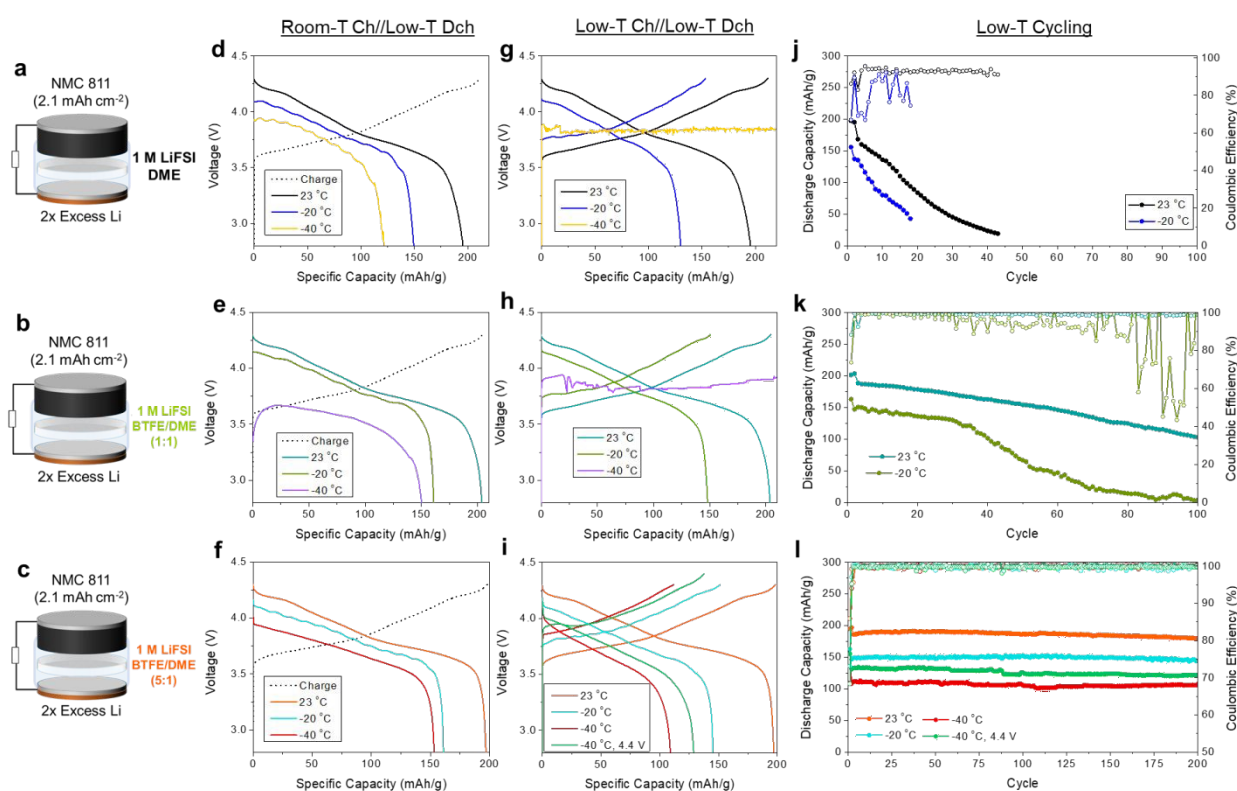


Figure 6. 2x Li||NMC 811 full cell operation at room and low temperature. Schematics of full cells employing **a**) 1 M LiFSI DME, **b**) 1 M LiFSI BTFE/DME (1:1), and **c**) 1 M LiFSI BTFE/DME (5:1) under flooded electrolyte conditions. 0.1 C rate discharge profiles of full cells charged at room temperature employing **d**) 1 M LiFSI DME, **e**) 1 M LiFSI BTFE/DME (1:1), and **f**) 1 M LiFSI BTFE/DME (5:1). Cycle profiles of full cells charged and discharged at various temperatures employing **g**) 1 M LiFSI DME, **h**) 1 M LiFSI BTFE/DME (1:1), and **i**) 1 M LiFSI BTFE/DME (5:1). All displayed voltage profiles represent the first available cycle post conditioning step. Cycling performance of full cells employing **j**) 1 M LiFSI DME, **k**) 1 M LiFSI BTFE/DME (1:1), and **l**) 1 M LiFSI BTFE/DME (5:1). Room temperature cycling was carried out at C/3||C/3 rates after 2 cycles at C/10 and low temperature cycling was carried out at C/10||C/5 for charge||discharge, respectively. Full cells were charged once at room temperature before transferring to low temperature.

331 Though a definitive causal understanding of temperature dependent Li metal plating has
332 not been reached, this work demonstrates that the introduction of ion-pairing in the electrolyte
333 results in vastly improved Li metal cycling at low temperatures. To provide a more practical
334 demonstration of these advantages, 2x excess Li||NMC 811 full cells were assembled and subjected
335 to a variety of performance tests at room and low temperatures. The 1 M LiFSI DME and 1 M
336 LiFSI BTFE/DME (1:1) systems were applied as SSIP-containing controls and compared to 1 M
337 LiFSI BTFE/DME (5:1) due to its relative balance between low temperature CE, critical current,
338 and oxidative stability (Figure 6a,b). Though the systems exhibiting an SSIP structure are sub-
339 optimal choices due to their reduced oxidative stability (Figure 2c, S2), such a comparison is
340 necessary to examine the influence of solvation structure on low temperature energy retention and
341 cyclability. These cells were assessed in two modes of operation: charging at room temperature
342 followed by a low temperature discharge, and both charging *and* discharging at the temperature of
343 interest. As shown in Figure 6d and 6e, the cells employing 1 M LiFSI DME and 1 M LiFSI
344 BTFE/DME (1:1) were found to output 195, 149, and 122 mAh g⁻¹ and 203, 163, and 154 mAh g⁻¹
345 (with respect to the cathode), respectfully when discharged at 23, -20, and -40 °C and after being
346 charged at room temperature. The relative increase in low temperature discharge capacity between
347 1 M LiFSI DME and the 1 M LiFSI BTFE/DME (1:1) system is possibly due to the increased CIP
348 character in the 1:1 mixture. Conversely, the 1 M LiFSI BTFE/DME (5:1) full cells displayed 197,
349 161, and 153 mAh g⁻¹ under the same conditions, indicative of improved electrochemical kinetics
350 over the controls despite significantly reduced bulk transport metrics (Figure 6f). Note that this
351 operation scheme does not involve Li plating at low temperature and thus shorting was
352 intentionally avoided.

353 High performance retention in the 5:1 electrolyte was also observed when subject to both
354 charge *and* discharge at reduced temperature, displaying discharge capacities of 145 and 109 mAh
355 g⁻¹ at -20 and -40 °C, respectively (Figure 6i). It is noteworthy that the ohmic polarization of
356 discharge at -40 °C is slightly improved compared to that which was charged at room temperature
357 (Figure 6f), which may be due to the higher surface area of Li, or variance of the SEI formed at
358 such temperatures.^[9] Additionally, it was found that this output capacity could be increased to 129
359 mAh g⁻¹ by increasing the cutoff voltage from 4.3 V to 4.4 V at -40 °C, which may partially
360 compensate for ohmic losses on the anode side at low temperature. This performance is not shared

361 by the 1 M LiFSI DME and 1 M LiFSI BTFE/DME (1:1) electrolyte cells under the same
362 conditions, which retained 130 and 147 mAh g⁻¹ when charged and discharged at -20 °C before
363 undergoing complete soft shorting at -40 °C. As previously discussed, we attribute these results to
364 the favorable temperature scaling of the charge-transfer process in ion-paired electrolytes, which
365 is consistent with 3-electrode impedance studies, which show a substantially reduced barrier for
366 the 5:1 electrolyte down to -40 °C for both the cathode and anode (Figure S14). These performance
367 results are consistent with the critical current results, and demonstrates that electrolytes which
368 exhibit SSIP structures are untenable for application in low temperature LMBs.

369 When subjected to cycling, the 1 M LiFSI DME full cells were found to be unable to retain
370 meaningful capacity, retaining 136 and 80 mAh g⁻¹ after 10 cycles at 23 and -20 °C, respectively
371 (Figure 6j). This performance is likely a combined effect of the poor oxidative stability of the
372 electrolyte, which may exacerbate transition metal dissolution on the cathode side, as well as the
373 comparatively poor Li reversibility of the 1 M LiFSI DME system.^[47] Full cells employing the 1:1
374 electrolyte retained 154 and 103 mAh g⁻¹ after 50 and 100 cycles at 23 °C, representing a
375 substantial improvement over the 1 M LiFSI DME electrolyte, which may be partially due to the
376 stability of the cathode electrolyte interphase (CEI) formed by BTFE (Figure S15). Hence, the 1
377 M LiFSI BTFE/DME (1:1) and provides a valid cycling baseline at ambient temperature to
378 examine the effect of solvation structure on low temperature performance. As predicted by the
379 previous trends (Figure 3), the poor Li metal cycling efficiency of the 1:1 electrolyte at -20 °C
380 (Figure 3b) was found to severely limit performance, where the output capacity significantly
381 decreased after 30 cycles, falling to 66 and 3.7 mAh g⁻¹ at the 50th and 100th cycle, respectively
382 (Figure 6k). On the other hand, the full cells employing 1 M LiFSI BTFE/DME (5:1) were found
383 to retain stable performance over 200 cycles without undergoing a meaningful reduction in output
384 capacity or coulombic efficiency that is generally associated with exhaustion of the Li metal anode
385 reservoir (Figure 6l).^[30] The capacity retention of these cells after 100 cycles were found to be
386 187, 153, 108, and mAh g⁻¹ at 23, -20, -40 (4.3 V cutoff), and -40 °C (4.4 V cutoff). The improved
387 performance of the 1 M LiFSI BTFE/DME (5:1) electrolyte is evidence that LMBs can be cycled
388 at low temperature reversibly without the need for thermal management.

389 To supplement the performance assessment of coin cells employing the electrolytes of
390 interest, scale-up projections were carried out to provide the expected energy density as a function

391 of temperature and operating scheme. The projections were based on 5 Ah pouch cells at an N/P
392 capacity ratio of 2 (2x excess Li) and a 3 g Ah⁻¹ electrolyte loading, with the specific capacities
393 and average voltages taken from the first cycle of the coin cell data (Figure S16). More details are
394 available in the Supporting Information. At a cathode loading of 2 mAh cm⁻², these projections
395 estimate that pouch cells employing 1 M LiFSI DME and charged at room temperature could
396 achieve energy densities of 303, 237, and 192 Wh kg⁻¹ whereas cells employing 1 M LiFSI
397 BTFE/DME (1:1) project to produce 309, 247, and 213 Wh kg⁻¹ at 23, -20, and -40 °C, respectively.
398 Under the same conditions, the 1 M LiFSI BTFE/DME (5:1) is expected to achieve 307, 250, and
399 230 Wh kg⁻¹. When both charged *and* discharged at the temperature of interest, the 1 M LiFSI
400 DME energy densities are expected to fall to 207, and 0 Wh kg⁻¹ (due to shorting) whereas 1 M
401 LiFSI BTFE/DME (1:1) are expected to fall to 226, and 0 Wh kg⁻¹ at -20 and -40 °C, respectively.
402 Conversely, the 5:1 electrolyte is expected to output 224, 163, and 194 Wh kg⁻¹ at -20, -40 (4.3 V
403 cutoff), and -40 °C (4.4 V cutoff), respectively. Additionally, increasing the cathode loading to 3
404 mAh cm⁻² in the 5:1 electrolyte under the same conditions is expected to increase these values to
405 342, 249, 181, and 216 Wh kg⁻¹ at 23, -20, -40 (4.3 V cutoff), and -40 °C (4.4 V cutoff),
406 respectively. Preliminary results indicate this optimization may be possible (Figure S17), however
407 the engineering of practical LMB pouch cells capable of low temperature cycling remains a
408 difficult task. If such a battery were realized at scale, the NASA 20LuSTR program goals of a >
409 250 Wh kg⁻¹ secondary battery operating at < -40 °C for over 100 cycles would be within reach.^[48]
410 While the electrolytes investigated here provide a scientific comparison of the effects of ion-
411 pairing on the temperature dependence of Li metal reversibility, it should be noted that electrolytes
412 employing solvents of a lower Li⁺ binding energy may improve the performance even further at
413 low temperatures.

414

415 Conclusions

416 A series of LHCE electrolytes composed of LiFSI, DME, and BFTE with varying local
417 concentrations were designed and compared to probe the effect of ion-pairing in the local solvation
418 structure on the low temperature performance of Li metal plating and stripping. It was found that
419 despite comparable room temperature performance, only systems with DME/Li⁺ molecular ratios

420 of 2.4 and below were capable of providing reversible Li cycling at -20 °C and below. What's
421 more, this performance trend was found to be in opposition to the ionic transport data, which
422 seemed to indicate that systems of low local concentration were superior. Through MD analysis,
423 it was found that this performance transition was coincident with a distinct shift in Li⁺ solvation
424 structure in which ion-pairing was a defining feature, and purely solvent dominated environments
425 were due to the lack of available DME molecules. Though this evidence is still correlational in
426 nature, previous reports indicate that ion-pairing may shift the balance of inner-sphere, which is
427 thought to be temperature independent, and outer-sphere reorganization energies such that low-
428 temperature performance is improved. Finally, 2x excess Li||NMC 811 full cells were assembled
429 utilizing both electrolytes of high and low local concentrations to demonstrate the translation of
430 these solvation effects during cell operation. Specifically, the cells employing electrolytes with
431 significant ion-pairing nature were able to demonstrate 100 cycles of reversible performance with
432 little capacity fade while retaining 63 % of their room temperature energy. This work
433 unambiguously demonstrates the positive effects of ion-paired solvation structures on the low
434 temperature Li metal reversibility while providing a viable route to LMBs charged *and* discharged
435 at low temperatures.

436 **Acknowledgements**

437 This work was supported by NASA Space Technology Graduate Research Opportunity
438 80NSSC20K1174. Z.C. acknowledges the support by an Early Career Faculty grant from NASA's
439 Space Technology Research Grants Program (ECF 80NSSC18K1512). The authors also
440 acknowledge the use of facilities and instrumentation supported by NSF through the UC San Diego
441 Materials Research Science and Engineering Center (UCSD MRSEC) DMR-2011924. Part of the
442 work used the UCSD-MTI Battery Fabrication Facility and the UCSD-Arbin Battery Testing
443 Facility. Electron microscopic characterization was performed at the San Diego Nanotechnology
444 Infrastructure (SDNI) of UCSD, a member of the National Nanotechnology Coordinated
445 Infrastructure, which is supported by the National Science Foundation (Grant ECCS-1542148).
446 This work also used the Extreme Science and Engineering Discovery Environment (XSEDE)^[49]
447 on the Expanse supercomputer at the San Diego Supercomputing center, which is supported by
448 National Science Foundation grant number ACI-1548562.

449

450 **Author Contributions**

451 J.H. conceived the original idea. P.L. and Z.C. directed the project. J.H., and K.K., carried out the
452 experiments. Y.Y., Z.W., H.L., and M.L. assisted with characterization. T.A.P directed the
453 computational experiments. J.H. and A.C. conducted computational experiments. H.G. and G.C.

454 assisted in experimental design and data processing. J.H., Z.C., P.L., and T.A.P wrote the paper.
455 All authors discussed the results and commented on the manuscript.

456

457 **Competing Interests**

458 The authors declare no competing interests.

459

460 **References**

- 461 [1] Gupta, A. & Manthiram, A. Designing Advanced Lithium-Based Batteries for Low-
462 Temperature Conditions. *Advanced Energy Materials* **2020**, 10, 2001972.
- 463 [2] Zhang, S. S.; Xu, K.; Jow, T. R. The Low Temperature Performance of Li-Ion Batteries.
464 *Journal of Power Sources* **2003**, 115 (1), 137–140.
- 465 [3] Smart, M. C.; Ratnakumar, B. V.; Chin, K. B.; Whitcanack, L. D. Lithium-Ion Electrolytes
466 Containing Ester Cosolvents for Improved Low Temperature Performance. *J. Electrochem.*
467 *Soc.* **2010**, 157 (12), A1361–A1374.
- 468 [4] Li, Q.; Jiao, S.; Luo, L.; Ding, M. S.; Zheng, J.; Cartmell, S. S.; Wang, C.-M.; Xu, K.; Zhang,
469 J.-G.; Xu, W. Wide-Temperature Electrolytes for Lithium-Ion Batteries. *ACS Appl. Mater.*
470 *Interfaces* **2017**, 9 (22), 18826–18835.
- 471 [5] Smart, M. C.; Ratnakumar, B. V.; Ewell, R. C.; Surampudi, S.; Puglia, F. J.; Gitzendanner, R.
472 The Use of Lithium-Ion Batteries for JPL's Mars Missions. *Electrochimica Acta* **2018**, 268,
473 27–40.
- 474 [6] Liu, J.; Bao, Z.; Cui, Y.; Dufek, E. J.; Goodenough, J. B.; Khalifah, P.; Li, Q.; Liaw, B. Y.;
475 Liu, P.; Manthiram, A.; Meng, Y. S.; Subramanian, V. R.; Toney, M. F.; Viswanathan, V.
476 V.; Whittingham, M. S.; Xiao, J.; Xu, W.; Yang, J.; Yang, X.-Q.; Zhang, J.-G. Pathways for
477 Practical High-Energy Long-Cycling Lithium Metal Batteries. *Nat Energy* **2019**, 4 (3), 180–
478 186.
- 479 [7] Xu, W.; Wang, J.; Ding, F.; Chen, X.; Nasybulin, E.; Zhang, Y.; Zhang, J.-G. Lithium Metal
480 Anodes for Rechargeable Batteries. *Energy Environ. Sci.* **2014**, 7 (2), 513–537.
- 481 [8] Li, S.; Jiang, M.; Xie, Y.; Xu, H.; Jia, J.; Li, J. Developing High-Performance Lithium Metal
482 Anode in Liquid Electrolytes: Challenges and Progress. *Advanced Materials* **2018**, 30 (17),
483 1706375.
- 484 [9] Thenuwara, A. C.; Shetty, P. P.; McDowell, M. T. Distinct Nanoscale Interphases and
485 Morphology of Lithium Metal Electrodes Operating at Low Temperatures. *Nano Lett.* **2019**,
486 19 (12), 8664–8672.
- 487 [10] Thenuwara, A. C.; Shetty, P. P.; Kondekar, N.; Sandoval, S. E.; Cavallaro, K.; May, R.;
488 Yang, C.-T.; Marbella, L. E.; Qi, Y.; McDowell, M. T. Efficient Low-Temperature Cycling
489 of Lithium Metal Anodes by Tailoring the Solid-Electrolyte Interphase. *ACS Energy Lett.*
490 **2020**, 5 (7), 2411–2420.

- 491 [11] Dong, X.; Lin, Y.; Li, P.; Ma, Y.; Huang, J.; Bin, D.; Wang, Y.; Qi, Y.; Xia, Y. High-
492 Energy Rechargeable Metallic Lithium Battery at $-70\text{ }^{\circ}\text{C}$ Enabled by a Cosolvent
493 Electrolyte. *Angewandte Chemie International Edition* **2019**, *58* (17), 5623–5627.
- 494 [12] Cheng, H.; Sun, Q.; Li, L.; Zou, Y.; Wang, Y.; Cai, T.; Zhao, F.; Liu, G.; Ma, Z.; Wahyudi,
495 W.; Li, Q.; Ming, J. Emerging Era of Electrolyte Solvation Structure and Interfacial Model
496 in Batteries. *ACS Energy Lett.* **2022**, *7* (1), 490–513.
- 497 [13] Hou, X.-K.; Li, S.-F.; Li, W.-H.; Liang, H.-J.; Gu, Z.-Y.; Luo, X.-X.; Wu, X.-L. Electrolyte
498 Chemistry Towards Improved Cycling Stability in Na-Based Dual-Ion Batteries with High-
499 Power/Energy Storage. *Batteries & Supercaps* **2021**, *4* (10), 1647–1653.
- 500 [14] Liang, H.-J.; Gu, Z.-Y.; Zhao, X.-X.; Guo, J.-Z.; Yang, J.-L.; Li, W.-H.; Li, B.; Liu, Z.-M.;
501 Li, W.-L.; Wu, X.-L. Ether-Based Electrolyte Chemistry Towards High-Voltage and Long-
502 Life Na-Ion Full Batteries. *Angewandte Chemie International Edition* **2021**, *60* (51), 26837–
503 26846.
- 504 [15] Rustomji, C. S.; Yang, Y.; Kim, T. K.; Mac, J.; Kim, Y. J.; Caldwell, E.; Chung, H.; Meng,
505 Y. S. Liquefied Gas Electrolytes for Electrochemical Energy Storage Devices. *Science* **2017**,
506 *356* (6345), eaal4263.
- 507 [16] Fan, X.; Ji, X.; Chen, L.; Chen, J.; Deng, T.; Han, F.; Yue, J.; Piao, N.; Wang, R.; Zhou, X.;
508 Xiao, X.; Chen, L.; Wang, C. All-Temperature Batteries Enabled by Fluorinated Electrolytes
509 with Non-Polar Solvents. *Nature Energy* **2019**, *4* (10), 882–890.
- 510 [17] Wang, C.-Y.; Zhang, G.; Ge, S.; Xu, T.; Ji, Y.; Yang, X.-G.; Leng, Y. Lithium-Ion Battery
511 Structure That Self-Heats at Low Temperatures. *Nature* **2016**, *529* (7587), 515–518.
- 512 [18] Ji, Y.; Wang, C. Y. Heating Strategies for Li-Ion Batteries Operated from Subzero
513 Temperatures. *Electrochimica Acta* **2013**, *107*, 664–674.
- 514 [19] Dong, X.; Guo, Z.; Guo, Z.; Wang, Y.; Xia, Y. Organic Batteries Operated at -70°C . *Joule*
515 **2018**, *2* (5), 902–913.
- 516 [20] Smart, M. C.; Lucht, B. L.; Dalavi, S.; Krause, F. C.; Ratnakumar, B. V. The Effect of
517 Additives upon the Performance of MCMB/LiNi_xCo_{1-x}O₂ Li-Ion Cells Containing Methyl
518 Butyrate-Based Wide Operating Temperature Range Electrolytes. *J. Electrochem. Soc.*
519 **2012**, *159* (6), A739–A751.
- 520 [21] Zhang, J.; Zhang, J.; Liu, T.; Wu, H.; Tian, S.; Zhou, L.; Zhang, B.; Cui, G. Towards Low-
521 Temperature Lithium Batteries: Advances and Prospects of Unconventional Electrolytes.
522 *Advanced Energy and Sustainability Research*. **2021**.
- 523 [22] Li, Q.; Lu, D.; Zheng, J.; Jiao, S.; Luo, L.; Wang, C.-M.; Xu, K.; Zhang, J.-G.; Xu, W. Li+-
524 Desolvation Dictating Lithium-Ion Battery's Low-Temperature Performances. *ACS Appl.*
525 *Mater. Interfaces* **2017**, *9* (49), 42761–42768.
- 526 [23] Holoubek, J.; Liu, H.; Wu, Z.; Yin, Y.; Xing, X.; Cai, G.; Yu, S.; Zhou, H.; Pascal, T. A.;
527 Chen, Z.; Liu, P. Tailoring Electrolyte Solvation for Li Metal Batteries Cycled at Ultra-Low
528 Temperature. *Nature Energy* **2021**, *6* (3), 303–313.

- 529 [24] Wang, Z.; Sun, Z.; Shi, Y.; Qi, F.; Gao, X.; Yang, H.; Cheng, H.-M.; Li, F. Ion-Dipole
530 Chemistry Drives Rapid Evolution of Li Ions Solvation Sheath in Low-Temperature Li
531 Batteries. *Advanced Energy Materials*. **2021**.
- 532 [25] Yamada, Y.; Wang, J.; Ko, S.; Watanabe, E.; Yamada, A. Advances and Issues in
533 Developing Salt-Concentrated Battery Electrolytes. *Nat Energy* **2019**, *4* (4), 269–280.
- 534 [26] Wang, J.; Yamada, Y.; Sodeyama, K.; Chiang, C. H.; Tateyama, Y.; Yamada, A.
535 Superconcentrated Electrolytes for a High-Voltage Lithium-Ion Battery. *Nature*
536 *Communications* **2016**, *7* (1), 12032.
- 537 [27] Fan, X.; Chen, L.; Ji, X.; Deng, T.; Hou, S.; Chen, J.; Zheng, J.; Wang, F.; Jiang, J.; Xu, K.;
538 Wang, C. Highly Fluorinated Interphases Enable High-Voltage Li-Metal Batteries. *Chem*
539 **2018**, *4* (1), 174–185.
- 540 [28] Chen, S.; Zheng, J.; Mei, D.; Han, K. S.; Engelhard, M. H.; Zhao, W.; Xu, W.; Liu, J.;
541 Zhang, J.-G. High-Voltage Lithium-Metal Batteries Enabled by Localized High-
542 Concentration Electrolytes. *Advanced Materials* **2018**, *30* (21), 1706102.
- 543 [29] Ren, X.; Zou, L.; Cao, X.; Engelhard, M. H.; Liu, W.; Burton, S. D.; Lee, H.; Niu, C.;
544 Matthews, B. E.; Zhu, Z.; Wang, C.; Arey, B. W.; Xiao, J.; Liu, J.; Zhang, J.-G.; Xu, W.
545 Enabling High-Voltage Lithium-Metal Batteries under Practical Conditions. *Joule* **2019**, *3*
546 (7), 1662–1676.
- 547 [30] Niu, C.; Lee, H.; Chen, S.; Li, Q.; Du, J.; Xu, W.; Zhang, J.-G.; Whittingham, M. S.; Xiao,
548 J.; Liu, J. High-Energy Lithium Metal Pouch Cells with Limited Anode Swelling and Long
549 Stable Cycles. *Nat Energy* **2019**, *4* (7), 551–559.
- 550 [31] Wang, J.; Huang, W.; Pei, A.; Li, Y.; Shi, F.; Yu, X.; Cui, Y. Improving Cyclability of Li
551 Metal Batteries at Elevated Temperatures and Its Origin Revealed by Cryo-Electron
552 Microscopy. *Nat Energy* **2019**, *4* (8), 664–670.
- 553 [32] Wang, H.; Kim, S. C.; Rojas, T.; Zhu, Y.; Li, Y.; Ma, L.; Xu, K.; Ngo, A. T.; Cui, Y.
554 Correlating Li-Ion Solvation Structures and Electrode Potential Temperature Coefficients. *J.*
555 *Am. Chem. Soc.* **2021**, *143* (5), 2264–2271.
- 556 [33] Ueno, K.; Yoshida, K.; Tsuchiya, M.; Tachikawa, N.; Dokko, K.; Watanabe, M. Glyme–
557 Lithium Salt Equimolar Molten Mixtures: Concentrated Solutions or Solvate Ionic Liquids?
558 *J. Phys. Chem. B* **2012**, *116* (36), 11323–11331.
- 559 [34] Ren, X.; Zou, L.; Jiao, S.; Mei, D.; Engelhard, M. H.; Li, Q.; Lee, H.; Niu, C.; Adams, B.
560 D.; Wang, C.; Liu, J.; Zhang, J.-G.; Xu, W. High-Concentration Ether Electrolytes for Stable
561 High-Voltage Lithium Metal Batteries. *ACS Energy Lett.* **2019**, *4* (4), 896–902.
- 562 [35] Fadel, E. R.; Faglioni, F.; Samsonidze, G.; Molinari, N.; Merinov, B. V.; Iii, W. A. G.;
563 Grossman, J. C.; Mailoa, J. P.; Kozinsky, B. Role of Solvent-Anion Charge Transfer in
564 Oxidative Degradation of Battery Electrolytes. *Nature Communications* **2019**, *10* (1), 3360.

- 565 [36] Adams, B. D.; Zheng, J.; Ren, X.; Xu, W.; Zhang, J.-G. Accurate Determination of
566 Coulombic Efficiency for Lithium Metal Anodes and Lithium Metal Batteries. *Advanced*
567 *Energy Materials* **8** (7), 1702097.
- 568 [37] Qian, J.; Henderson, W. A.; Xu, W.; Bhattacharya, P.; Engelhard, M.; Borodin, O.; Zhang,
569 J.-G. High Rate and Stable Cycling of Lithium Metal Anode. *Nature Communications* **2015**,
570 **6**, 6362.
- 571 [38] Marcus, R. A. On the Theory of Electron-Transfer Reactions. VI. Unified Treatment for
572 Homogeneous and Electrode Reactions. *J. Chem. Phys.* **1965**, *43* (2), 679–701.
- 573 [39] Newton, M. D.; Sutin, N. Electron Transfer Reactions in Condensed Phases. *Annual Review*
574 *of Physical Chemistry* **1984**, *35* (1), 437–480.
- 575 [40] Chidsey, C. E. D. Free Energy and Temperature Dependence of Electron Transfer at the
576 Metal-Electrolyte Interface. *Science* **1991**, *251* (4996), 919–922.
- 577 [41] Derr, D. L.; Elliott, C. M. Temperature Dependence of the Outer-Sphere Reorganization
578 Energy. *J. Phys. Chem. A* **1999**, *103* (39), 7888–7893.
- 579 [42] Nazmutdinov, R.; Quaino, P.; Colombo, E.; Santos, E.; Schmickler, W. A Model for the
580 Effect of Ion Pairing on an Outer Sphere Electron Transfer. *Phys. Chem. Chem. Phys.* **2020**,
581 *22* (25), 13923–13929.
- 582 [43] Perez Beltran, S.; Cao, X.; Zhang, J.-G.; Balbuena, P. B. Localized High Concentration
583 Electrolytes for High Voltage Lithium–Metal Batteries: Correlation between the Electrolyte
584 Composition and Its Reductive/Oxidative Stability. *Chem. Mater.* **2020**, *32* (14), 5973–
585 5984.
- 586 [44] Boyle, D. T.; Kong, X.; Pei, A.; Rudnicki, P. E.; Shi, F.; Huang, W.; Bao, Z.; Qin, J.; Cui,
587 Y. Transient Voltammetry with Ultramicroelectrodes Reveals the Electron Transfer Kinetics
588 of Lithium Metal Anodes. *ACS Energy Lett.* **2020**, *5* (3), 701–709.
- 589 [45] Huang, B.; Myint, K. H.; Wang, Y.; Zhang, Y.; Rao, R. R.; Sun, J.; Muy, S.; Katayama, Y.;
590 Corchado Garcia, J.; Fraggadakis, D.; Grossman, J. C.; Bazant, M. Z.; Xu, K.; Willard, A. P.;
591 Shao-Horn, Y. Cation-Dependent Interfacial Structures and Kinetics for Outer-Sphere
592 Electron-Transfer Reactions. *J. Phys. Chem. C* **2021**, *125* (8), 4397–4411.
- 593 [46] Baskin, A.; Lawson, J. W.; Prendergast, D. Anion-Assisted Delivery of Multivalent Cations
594 to Inert Electrodes. *J. Phys. Chem. Lett.* **2021**, *12* (18), 4347–4356.
- 595 [47] Asl, H. Y.; Manthiram, A. Reining in Dissolved Transition-Metal Ions. *Science* **2020**, *369*
596 (6500), 140–141.
- 597 [48] National Aeronautics and Space Administration. Space Technology Research Grants, Lunar
598 Surface Technology Research Opportunities Appendix. **2020**.
- 599 [49] Towns, J.; Cockerill, T.; Dahan, M.; Foster, I.; Gaither, K.; Grimshaw, A.; Hazlewood, V.;
600 Lathrop, S.; Lifka, D.; Peterson, G. D.; Roskies, R.; Scott, J. R.; Wilkins-Diehr, N. XSEDE:
601 Accelerating Scientific Discovery. *Computing in Science Engineering* **2014**, *16* (5), 62–74.